Development of Pd-supported Catalysts for the Conversion of Palm Oil to Biohydrogenated Diesel in a Microscale-based Reactor

Y. Sa-ngasaeng,[a] R. Nernrimnong,[a] N. Sirimungkalakul,[b] G. Jovanovic,[c] and S. Jongpatiwut[a,d,*]

[a]The Petroleum and Petrochemical College, Chulalongkorn University, Bangkok 10330, Thailand

[b]Innovation Institute, PTT Public Company Limited, Ayutthaya 13170, Thailand

[c]School of Chemical, Biological, and Environmental Engineering, Oregon State University, Corvallis, OR 97331, USA

[d]Center of Excellence on Petrochemical and Materials Technology, Chulalongkorn University, Bangkok 10330, Thailand

doi: https://doi.org/10.15255/CABEQ.2020.1893

Original scientific paper
Received: November 17, 2020
Accepted: March 5, 2021

In this research, the preparation of Pd-supported catalysts in microreactor was investigated for the production of renewable biohydrogenated diesel (BHD). Pd/Al_2O_3 and Pd/TiO_2 catalysts were prepared by two different coating methods, slurry suspension (SUS), and sol-gel method (SG). Catalysts were coated on microreactor walls and tested for the deoxygenation of palm oil to BHD at 325 ºC, 3.4 MPa, H_2/feed molar ratio of 96. The coated catalysts were characterized by several techniques, including 3D-optical profiler, SEM-EDX, XRD, BET, and adhesion test. The experimental results show that SUS method provided a homogeneous catalyst layer, while the SG method gave a non-homogeneous cracked coating. In terms of catalytic activity, Pd/TiO_2 (SG) exhibited the highest space-time yield (STY) of BHD (g BHD g^{-1} catalyst h^{-1}), which could be due to its unique characteristics of pure anatase phase and strong metal-support interaction for hydrogen spillover mechanism.

Keywords:
deoxygenation, catalyst coating, biohydrogenated diesel, microscale-based reactor

Introduction

Microstructured reactors have emerged as an innovative platform technology for process intensification, which involves a substantial improvement in equipment size, energy consumption, costs, and safety. The microscale-based reactors give high surface to volume ratio $10^4 – 10^7$ $m^2_{cat\text{-}surface}/m^3_{reactor\ volume}$ compared to conventional reactors (approximately 10^2 $m^2_{cat\text{-}surface}/m^3_{reactor\ volume}$).[1,2] These reactors allow reactants to flow in a thin film between reactor walls (100 – 1000 μm apart), resulting in the superior heat and mass transfer rate and reduction of hot-spot during operation.[1,3] Microscale-based reactors are suitable for operation with highly endothermic or exothermic, and even explosive reaction processes.[4,5] Other advantages are short residence times, narrow residence time distributions, higher space-time yield, lower energy consumption, and lower capital cost.[1,6–8] Furthermore, microscale-based reactors have an effective way of increasing the capacity of production by numbering-up the units with the identical design.[9,10]

There are several applications for catalytic reaction systems in microscale-based reactor, such as hydrogenation, oxidation process, Fischer-Tropsch synthesis, methanol synthesis, steam reforming, dehydration of alcohols, epoxide synthesis, and photocatalytic process.[7,11–15] These reaction processes are often supported with thin (~1 μm) solid-catalyst layers coated on the microreactor walls.[13] The transesterification process in microreactor has been widely studied.[16–19] However, there are only few studies[3,20–22] about hydrodeoxygenation of triglycerides to produce liquid fuel in the microreactor. One noted challenge in the process of hydrodeoxygenation of vegetable oils in packed bed reactors is a limited mass transfer between gas, liquid, and solid catalyst phase. Limited mass transfer is primarily caused by a very low diffusion coefficient for bulky molecules of triglycerides.[3] In one study, Sinha and co-worker[3] studied the hydroprocessing of jatropha oil to kerosene and diesel over $NiMo/Al_2O_3$

*Corresponding author: E-mail: siriporn.j@chula.ac.th

catalyst using microchannel, and monolithic reactors. The results showed that reaction selectivity had improved when compared to the conventional trickle bed reactor. Another study by Zhou *et al.*[20] investigated the hydrodeoxygenation of microalgae oil to green diesel using pre-sulfided $NiMo/Al_2O_3$ catalyst in micro fixed-bed reactor. They found that the space-time yield (STY) of product had enhanced in a microreactor (internal diameter < 1 mm) when compared to macroscopic reactor (internal diameter > 1 mm) because of the microreactor's superior mass transfer characteristics. The extraordinary mass transport performance of microscale-based reactors is best viewed by rivalling the characteristic diffusion times in a typical microreactor (t_{dif} = 10–100 ms) and classic reactors (t_{dif} = 10,000–100,000 ms).

One of the challenges in heterogeneous catalytic reaction processes in a microscale-based reactor, is the coating of catalyst on the reactor walls.[23] To achieve a long-term stability of the catalyst coating, a strong adhesion between catalyst and the substrate is desired.[13] To improve the coating adhesion, a thermal pretreatment was used to create an oxide layer before catalyst coating was applied.[24] While there are several methods to coat the catalyst on the surface of reactors (suspension, sol-gel deposition, hybrid method between suspension and sol-gel, electrophoretic deposition (EPD), chemical vapor deposition (CVD), and physical vapor deposition (PVD)[14,24–26]), the suspension and the sol-gel methods are the most widely used.[14,24] Suspension method is a simple technique that uses a slurry of the catalyst support (Al_2O_3, TiO_2) or finished catalyst, binder, acid, and solvent (water) as main ingridients.[14,24,27] Sol-gel method is a low-temperature process, in which a small amount of precursor is used.[28,29] Sol-gel coating method provides a thinner layer than the suspension method.[24] The suspension and sol-gel solutions are typically coated on reactor walls by washcoating, dip-coating, or spray coating procedures.

In the hydrodeoxygenation process, noble-metal catalysts are considered more active and more environmentally favorable than sulfided transition metal catalysts.[30,31] Palladium (Pd) is one of the noble metals with high catalytic performance for hydrogenation reaction.[31,32] A Pd-supported titania (TiO_2) catalyst showed high catalytic activity for biohydrogenated diesel production.[33] An alternative catalyst support, alumina (Al_2O_3), is also widely used as a catalyst support in the hydrotreating process of vegetable oils.[20,34,35] In this study, comparison of catalytic activity of Pd supported by alumina or titania, prepared by two different coating slurries (suspension and sol-gel), is a point of interest in our investigation. The physical and chemical properties of the coated catalysts were analyzed by 3D-optical profiler measurement, SEM-EDX, XRD, BET, and adhesion test. The catalytic activity in the microscale-based reactor was tested for converting vegetable oil to biohydrogenated diesel at 325 ºC, 3.4 MPa, and H_2/feed molar ratio of 96.

Material and methods

Microscale-based reactor

Experiments were performed in a microscale-based reactor with dimensions of 30 cm x 20 cm x 5 cm (PCT patent application No. PCT/US2016/061814, United States: 15/774,756, Japan: JP2018-525363, Thailand: 1801002705). Fig. 1 shows the design of the experimental microscale-based rector, a) 3D 'exploded' view of the reactor, b) top view of the catalyst plate, c) cross-section view of catalyst holder with the coated catalyst on the substrate plate, and d) top view of bottom clamp plate. The catalyst plate (14.5 cm x 18 cm) was made of stainless steel 316 with a multitude of 300 μm high microposts. The diameter of microposts was 300 μm, and microposts were arranged in an equilateral (1 mm) triangular pitch. The assembly of two catalyst plates generated 600 μm size of microscale-base reactor. The complete experimental assembly consisted of two catalyst plates, two mixer stainless steel plates, and two cover plates. All plates were laser welded to provide excellent sealing and plate alignments (Fig. 1c). The catalyst holder was put into the bottom clamp plate. Afterward, the bottom clamp plate was assembled with the top clamp plate using a graphite seal and tightened with 18 screws (Fig. 1d).

Catalyst preparation

Catalyst plate pretreatment

Before catalyst coating, the catalyst plates were pretreated by rinsing with DI water, followed by ethanol rinse to remove impurities from the plate. The plate was then sonicated in 20 wt% citric acid ($C_6H_8O_7 \cdot H_2O$, RCI Labscan Limited) for 30 min, dried, and calcined in a furnace at 800 ºC for 2 h in the air environment. This thermal treatment of the SS catalyst plates creates a thin oxide layer, which substantially improves the catalyst adhesion.

Washcoating of alumina catalyst support

Alumina support was coated on catalyst plate by washcoating of the alumina slurry. The slurry was prepared by suspension (SUS) or sol-gel (SG) method. For suspension, polyvinyl alcohol (PVA, 98–99 % hydrolyzed, Polysciences) was slowly dissolved in hot water at 85 ºC and continuously stirred for 3 h. Acetic acid (CH_3COOH, 100 %, QReC) was then

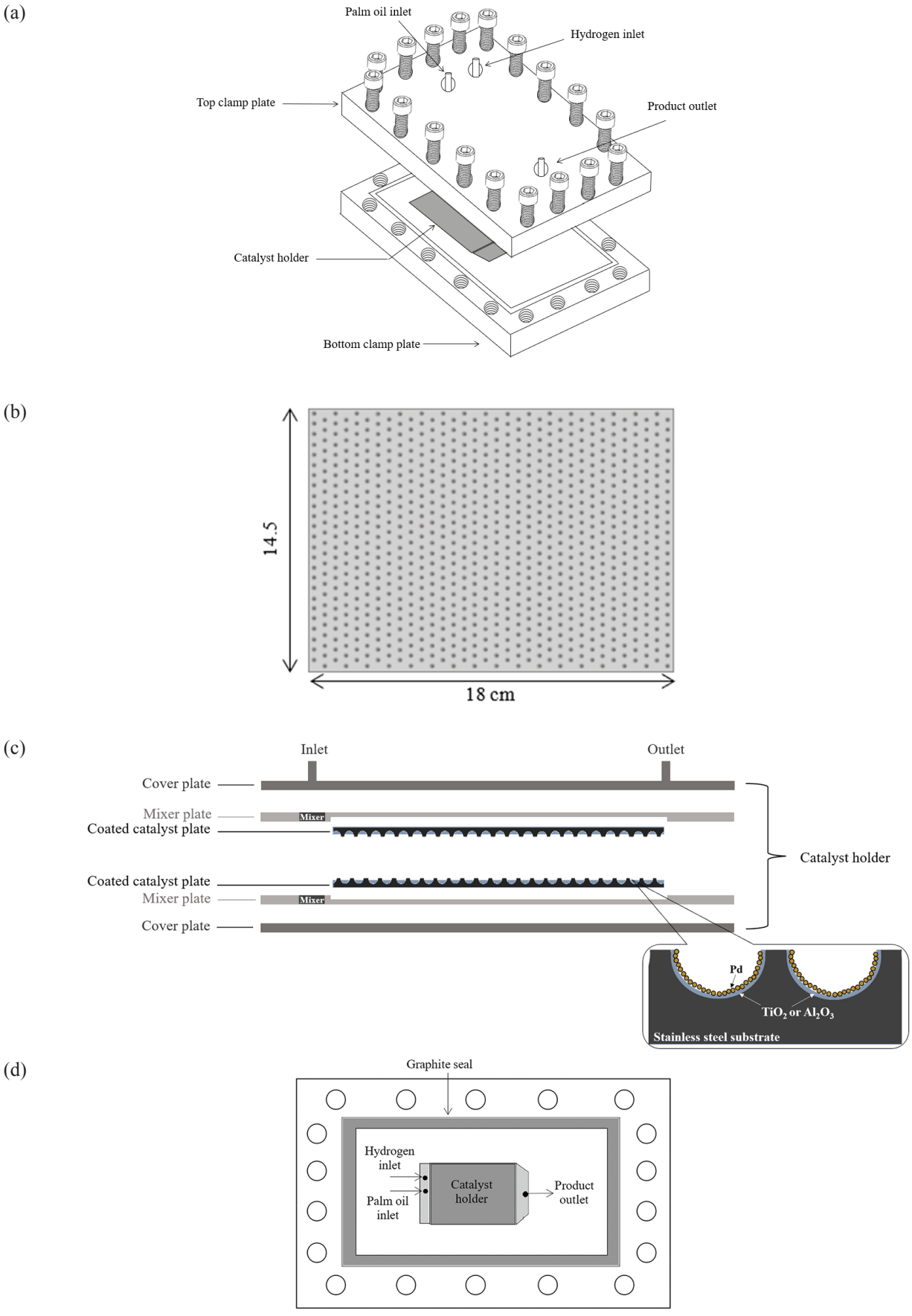

F i g . 1 – *Schematic of microscale-based reactor design: (a) three-dimensional view, (b) top view of catalyst plate, (c) cross-section view of catalyst holder with the coated catalyst on the substrate plate, and (d) top view of bottom clamp plate*

added to the solution, followed by aluminum oxide powder (Al_2O_3, Dispersal HP14, SASOL) and stirred for 3 h. The mass fractions of Al_2O_3: CH_3COOH: H_2O: PVA were 10:1:100:5. The suspension was used to coat the pretreated catalyst plate by the washcoating method. The washcoated suspension on catalyst plate was then dried at 110 ºC overnight, followed by calcination in air at 500 ºC for 4 h with a heating ramp rate of 10 ºC min^{-1}. For the sol-gel method, DI water and ethanol (EtOH, C_2H_6O, 99.9 %, Merck) were mixed and stirred at 45 ºC for 15 min. Afterward, aluminum isopropoxide (AIP, Aldrich) was added gradually, and continuously stirred at 80 ºC for 45 min, followed by adding aluminum acetylacetonate (AlAcAc, Aldrich) and PVA. The molar ratio of the components AIP: H_2O: EtOH: AlAcAc was 1:100:10:0.5 with 3 wt% PVA as a binder. Nitric acid (HNO_3, 70 %, Ajax Finechem) was then added in the alumina sol until pH equaled 4. The solution was stirred at 80 ºC for 24 h resulting in a homogeneous solution. The pretreated catalyst plates were coated by sol-gel solution, dried at room temperature for 5 h, and then oven-dried at 100 ºC overnight, followed by calcination at 600 ºC in air for 2 h with a heating ramp rate of 2 ºC min^{-1}.[3]

Washcoating of titania catalyst support

Titania support was also coated on pretreated catalyst plate by washcoating method using titania slurries prepared by suspension or sol solution from the sol-gel method. For the suspension, the slurry was prepared by the same procedure as alumina, except using nanopowder titania (P25, 21 nm, Sigma-Aldrich). After the washcoating, the sample was dried in an oven at 110 ºC overnight, followed by calcination at 500 ºC in air for 4 h with a heating ramp rate of 10 ºC min^{-1}.

For the sol-gel method preparation, acetylacetone (ACA, Merck) was homogeneously mixed with tetra isopropyl titanate (TIPT, Aldrich) with a 1:1 molar ratio. Afterward, a laurylamine hydrochloride (LAHC, 98 %, Merck) aqueous solution with a pH of 4.2 was prepared by mixing LAHC with ethanol and distilled water (3:2 volume ratio) and hydrochloric acid (HCl, 37 %, RCI Labscan). The prepared LAHC aqueous solution was added to the ACA-modified TIPT solution, in which the molar ratio of TIPT to LAHC was 4 to control the porosity of TiO_2. The mixture was continuously stirred at room temperature overnight to obtain transparent yellow sol as a homogeneous sol solution.[33] The solution was coated onto a pretreated plate, then dried at 80 ºC in a closed system for 3 h to complete gel formation. The coated plates with gel were dried in the open system at the same temperature (80 ºC) overnight to evaporate water, followed by calcination at 500 ºC in air for 4 h with a heating ramp rate of 10 ºC min^{-1} to remove the LAHC template.

Impregnation of Pd

The inclusion of Pd on Al_2O_3 and TiO_2 coated films on the catalyst plate was done by the im pregnation method. Palladium nitrate dihydrate ($Pd(NO_3)_2 \cdot 2H_2O$, Aldrich) solution was added to the coated Al_2O_3 or TiO_2 support to acquire the 1 wt% of Pd loading. After impregnation, the coated plates were dried at 110 ºC overnight, followed by calcination at 500 ºC in air for 4 h with a heating ramp rate of 10 ºC min^{-1}.

Catalyst preparation for fixed bed reactor

The TiO_2 support was prepared by the sol-gel method. After obtaining transparent yellow sol, the sol was dried at 80 ºC in a closed system for a week to complete the gel formation. Subsequently, the gel was dried in air at 80 ºC overnight, and calcined at 500 ºC for 4 h to obtain TiO_2 support powder. The incorporation of 1 wt% Pd on TiO_2 powder was prepared by the incipient wetness impregnation method. The Pd/TiO_2 catalyst was then pelletized and sieved to obtain 20–40 mesh of particle size before placing it in a fixed bed reactor.

Catalyst characterization methods

The prepared catalysts were tested for their physical and chemical properties. The coated catalyst plates were analyzed for their morphology, composition, and adhesion by scanning electron microscope (SEM), energy-dispersive X-ray analysis (EDX), 3D optical profiler measurement, and adhesion test. SEM-EDX (JEOL JSM-6610LV) provides the catalyst layer coating images and elemental composition results. The 3D optical profiler and surface measurement using ZeGage machine provide measurements of the surface texture, roughness, and thickness of catalyst layer. The adhesion between the coated catalyst and catalyst plate was evaluated by weight remaining after sonication in dodecane using an ultrasonic bath (Elma, 25 kHz and 750 W) for 30 min, as defined in the following equation.

$$\text{Adhesion (\%)} = \frac{\text{weight of catalyst after sonication}}{\text{weight of catalyst before sonication}} \cdot 100 \quad (1)$$

For Brunauer-Emmett-Teller (BET) surface determination and X-ray diffraction (XRD) analysis, the catalyst sample was detached from the plate and provided in powder form. The BET surface area analyzer (BEL, Belsorp Mini-II) was used to analyze the impregnated Pd catalyst's surface area. The samples were outgassed under vacuum condition at 350 ºC for 4 h before analysis. The XRD analysis method was used to identify the crystalline material by Rigaku X-ray diffractometer system (RINT-

2200) with CuK α radiation (1.5406 Å) and a nickel filter. The catalysts were measured in the 2θ range of 20–80º with a scanning speed of 5º min^{-1}.

Catalyst activity testing

The catalyst was activated before testing. Two catalyst plates were installed and sealed with two mixing plates and two cover plates, as shown in Fig. 1c. The assembled reactor was placed in a furnace at 200 ºC and exposed to a flow of 99.99 % of hydrogen for three hours. The stream of 50 wt% of palm oil in dodecane was then fed to the reactor using a high-pressure pump (Waters 515). The flow of hydrogen gas and the reaction pressure were controlled by a mass flow controller (Brooks, SLA5800 Series) and a backpressure regulator (Brooks, SLA5800 Series). The reaction was performed at 325 °C, 3.4 MPa, H_2/feed molar ratio of 96, and WHSV of 4.6, 9.7, 15.8, and 27.9 h^{-1}. The liquid product was separated by a gas-liquid separator, and analyzed hourly by an Agilent 7890A gas chromatograph equipped with an FID detector, as illustrated in Fig. 2.

For the conventional fixed bed reactor operation, the catalyst pellets were reduced by flowing 99.99 % hydrogen at 200 °C for three hours. The stream of pure palm oil was fed to the reactor (3/4-inch OD, stainless steel) with a flow of hydrogen at an H_2/feed molar ratio of 30. The reaction was operated at 325 °C, 3.4 MPa, and WHSV of 0.7 h^{-1}. The liquid product was collected in a condenser, and analyzed by a gas chromatograph equipped with an FID detector (Agilent 7890A). The conversion and space-time yield were calculated using Eq. 2 and Eq. 3:

Conversion:

$$\text{Conversion (\%)} = \frac{\text{weight of feed converted}}{\text{weight of feed input}} \cdot 100 \quad (2)$$

Space-time yield:

$$\text{STY} = \frac{\text{weight of BHD produced/time}}{\text{weight of catalyst}} \quad (3)$$

Results and discussion

Surface morphology of catalyst plates

To improve the adhesion between the catalyst and catalyst plate, the catalyst plates were thermally pretreated to increase surface roughness and generate an oxide layer.[36,37] The catalyst plates before and after pretreatment with citric acid followed by thermal pretreatment were analyzed for their surface morphology using SEM-EDX and 3D-optical profiler measurement. Table 1 summarizes surface roughness and elemental composition of catalyst plate before and after pretreatment. The results showed that the surface roughness of the catalyst plate before pretreatment and catalyst plate cleaned with citric acid was not significantly different. In contrast, the roughness increased from 3.055 μm to 3.283 μm after thermal pretreatment. Fig. 3 shows

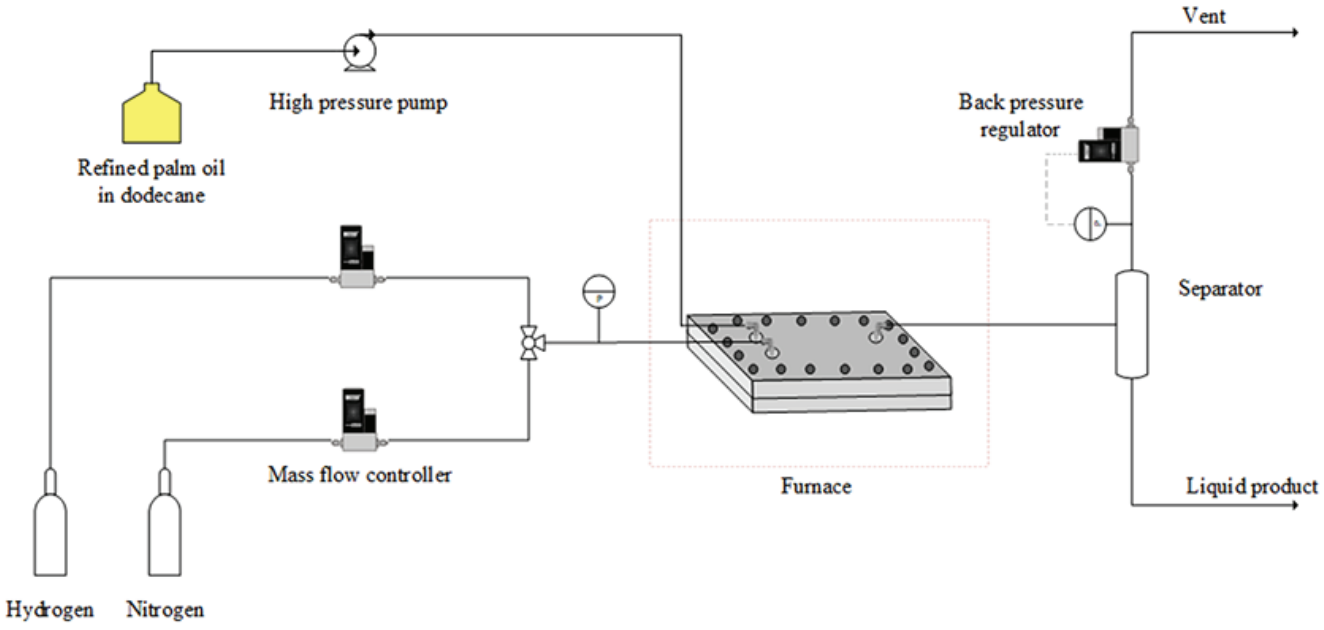

Fig. 2 – *Schematic flow diagram of microscale-based reactor set*

Table 1 – *Surface roughness and elemental composition (wt%) of catalyst plate before and after pretreatment*

	Surface roughness/μm[a]	Element/wt%[b]							
		C	O	Si	Cr	Mn	Fe	Ni	Mo
Catalyst plate before pretreatment	3.050	4.38	7.71	1.05	18.06	1.04	56.42	7.77	3.56
Catalyst plate after citric acid cleaning	3.055	n.a.	n.a.	n.a.	n.a.	n.a.	n.a.	n.a.	n.a.
Catalyst plate after thermal pretreatment	3.283	3.65	36.05	0.14	5.07	2.45	48.69	3.15	0.80

[a]Analyzed by 3D-optical profiler measurement.

[b]Analyzed by SEM-EDX.

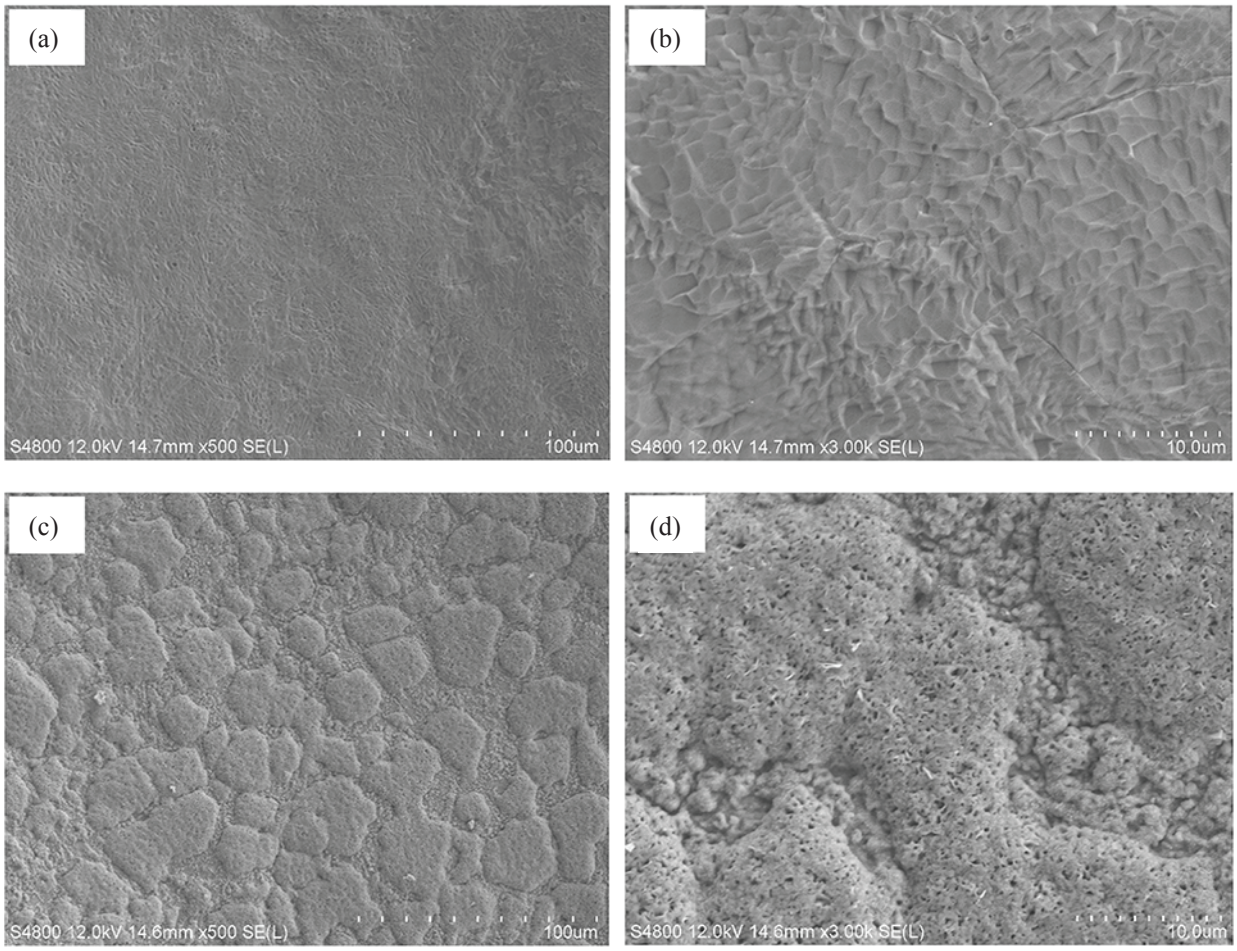

Fig. 3 – *SEM images of catalyst plates: (a) before pretreatment (x500), (b) before pretreatment (x3,000), (c) after thermal pretreatment (x500), and (d) after thermal pretreatment (x3,000)*

SEM images of the catalyst plate before and after thermal pretreatment at a magnification of 500 and 3,000. The surface morphology of catalyst plate before pretreatment was smooth compared to the one after thermal pretreatment. The contents of oxygen increased after thermal pretreatment from 7.71 wt% to 36.05 wt%, while the composition of other elements relatively decreased. The SEM images (Fig. 3c) and elemental composition suggests the presence of iron oxide layer with higher roughness after thermal pretreatment. Similar effects were reported by Schmidt *et al.*[27] The thermal pretreatment enhances adhesion between the catalyst layer and catalyst plate due to increasing anchoring sites on the stainless-steel surface caused by iron oxide layer formation.[38,39]

Coated catalyst characterization

The morphology and thickness of the catalyst layer on the catalyst plate was investigated by 3D optical profiler measurement. Fig. 4 illustrates 3D optical images of a blank catalyst plate, and catalyst plates coated with Pd/Al_2O_3 (SUS), Pd/Al_2O_3 (SG), Pd/TiO_2 (SUS), and Pd/TiO_2 (SG), respectively. The

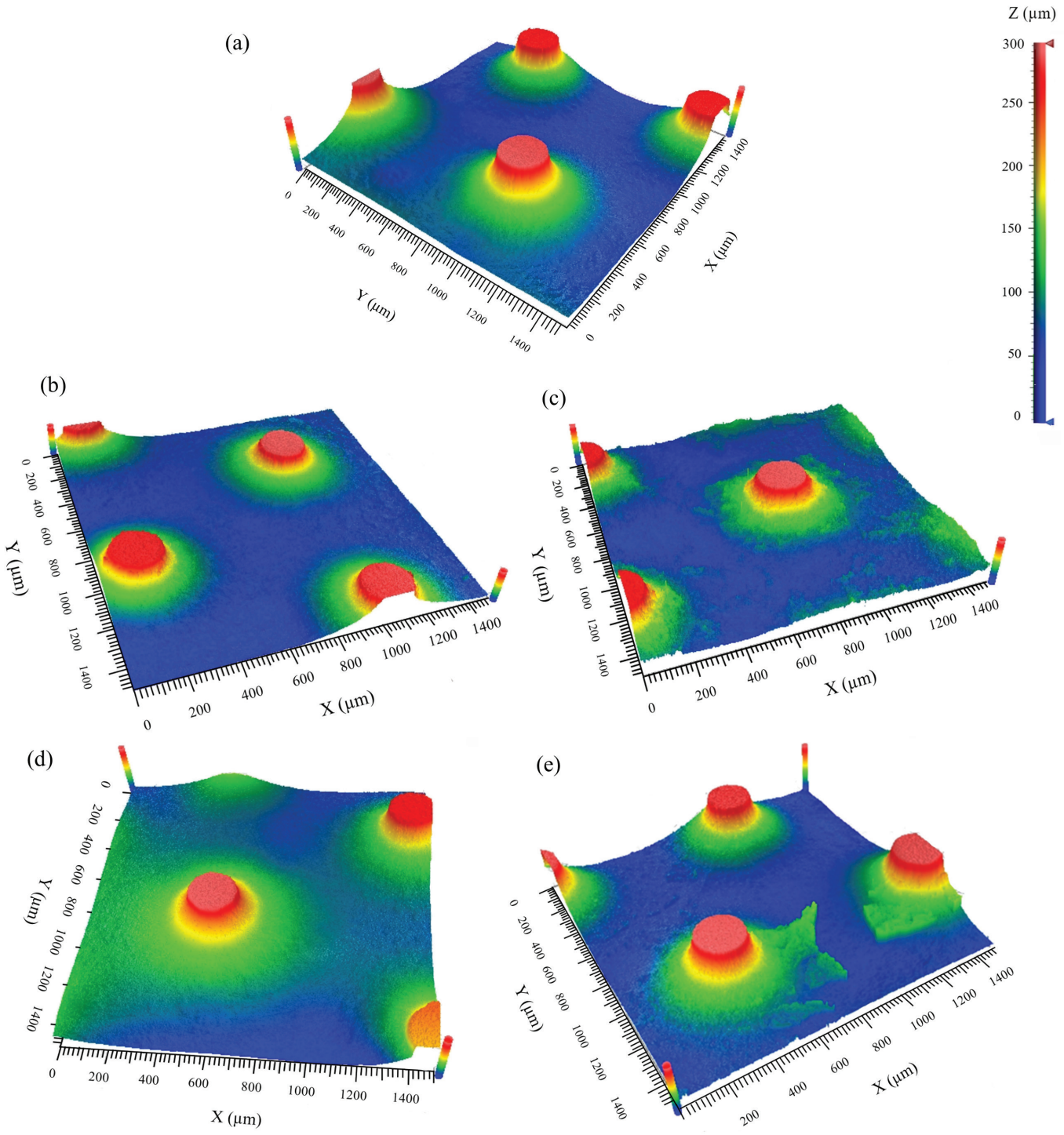

Fig. 4 – *3D optical images of different catalysts on catalyst plate: (a) blank catalyst plate, (b) Pd/Al_2O_3 (SUS), (c) Pd/Al_2O_3 (SG), (d) Pd/TiO_2 (SUS), and (e) Pd/TiO_2 (SG)*

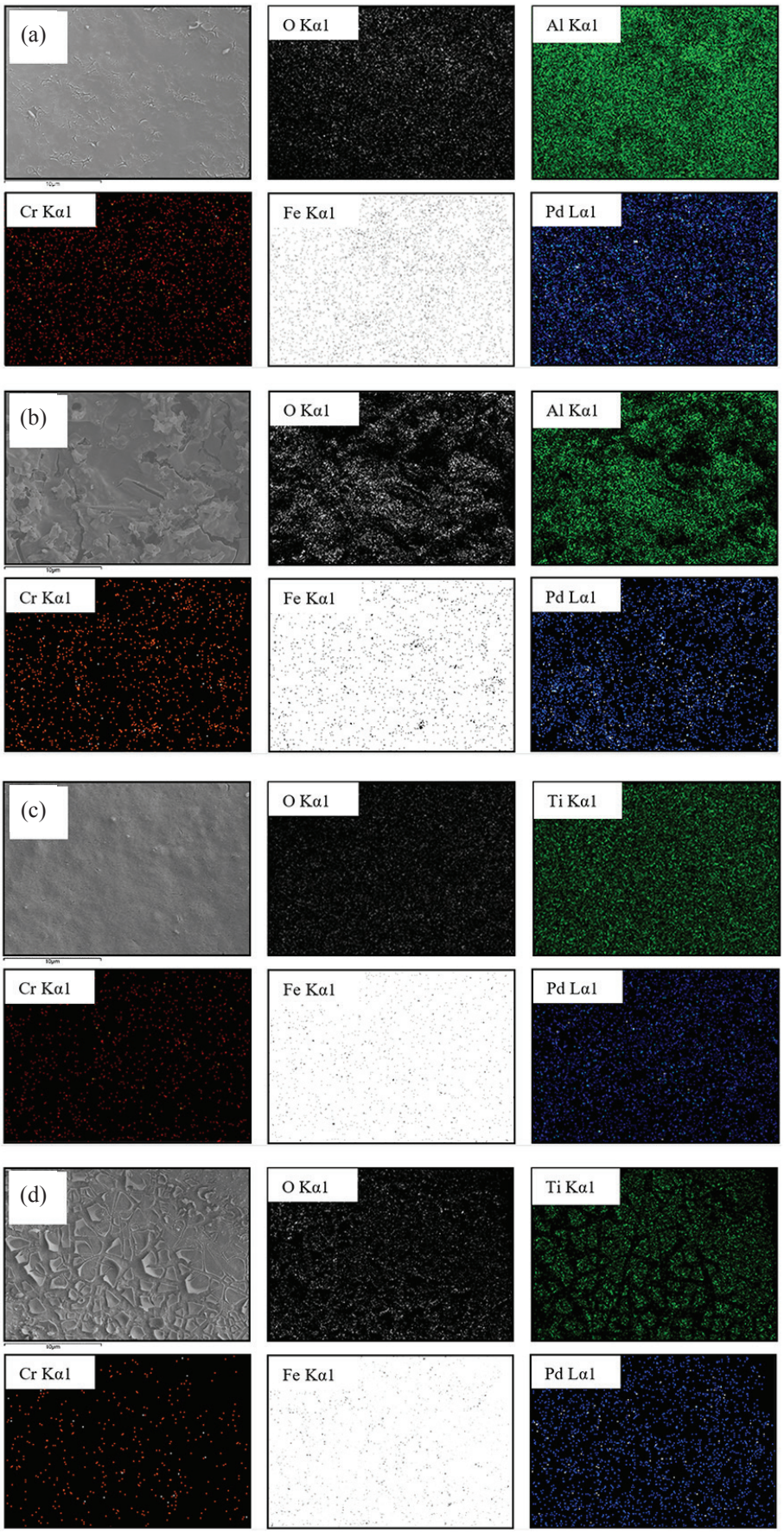

Fig. 5 – *SEM images and SEM-EDX mapping of different catalysts on the catalyst plate: (a) Pd/Al_2O_3 (SUS), (b) Pd/Al_2O_3 (SG), (c) Pd/TiO_2 (SUS), and (d) Pd/TiO_2 (SG)*

Table 2 – *Quantity, thickness, surface area, calculated WHSV, and %adhesion of the prepared Pd-supported catalysts*

Catalyst	Quantity/g[a]	Thickness/μm[b]	Surface area/(m^2 g^{-1} catalyst)[c]	Calculated WHSV/h^{-1}	% Adhesion
Pd/Al_2O_3 (SUS)	1.03	17–20	142	4.6	83.05
Pd/Al_2O_3 (SG)	0.49	25–28	243	9.7	82.74
Pd/TiO_2 (SUS)	0.32	44–47	40	15.8	87.94
Pd/TiO_2 (SG)	0.17	34–38	63	27.9	30.19

[a]Quantity of catalyst on the catalyst plate.

[b]Analyzed by 3D-optical profiler measurement.

[c]Brunauer-Emmett-Teller (BET) surface area.

thickness and quantity of catalysts are summarized in Table 2. Fig. 4a shows the 3D optical profile images of a blank catalyst plate whose microposts height are 300 μm. Fig. 4b shows that the coated Pd/Al_2O_3 (SUS) catalyst was thin and uniform. In contrast, the coated Pd/Al_2O_3 (SG) catalyst (Fig. 4c) was thick and uneven on the catalyst plate. The thickness of Pd/Al_2O_3 (SUS) was 17–20 μm, which was lower than Pd/Al_2O_3 (SG) (25–28 μm). On the other hand, the quantity of Pd/Al_2O_3 (SUS) on the catalyst plate was higher than Pd/Al_2O_3 (SG), which could be due to the high density of Al_2O_3 commercial powder used in suspension method. As shown in Fig. 4d, the Pd/TiO_2 (SUS) provided a thick, uniform and smooth layer on the catalyst plate. It was observed from Fig. 4e that the Pd/TiO_2 (SG) presented a non-uniform and cracked layer on the surface. In agreement with 3D optical profile results, the thickness of the Pd/TiO_2 (SUS) catalyst layer was 44–47 μm, which was higher than that of Pd/TiO_2 (SG) (34–38 μm). In line with the thickness, the Pd/TiO_2 (SUS) weight was higher than Pd/TiO_2 (SG).

SEM-EDX confirmed the morphology and elemental distribution of catalysts. Fig. 5 exhibits SEM images and SEM-EDX mapping results of different catalysts on the catalyst plate, which are Pd/Al_2O_3 (SUS), Pd/Al_2O_3 (SG), Pd/TiO_2 (SUS), and Pd/TiO_2 (SG), respectively. In agreement with 3D optical profile results, the SEM images in Figs. 5a and 5c indicate that the Pd/Al_2O_3 (SUS) and Pd/TiO_2 (SUS) catalysts gave a uniform and homogeneous layer. The corresponding EDX results also show a high distribution of support composition (Al or Ti and O) on the catalyst plate. This could be due to the narrow particle size distribution of Al_2O_3 and TiO_2 powder (<50 nm) used in the suspension slurry. As shown in Figs. 5b and 5d, the SEM images of Pd/Al_2O_3 (SG) and Pd/TiO_2 (SG) gave a cracked non-continuous layer, and some agglomeration as also observed by 3D optical profile images. The EDX mapping of Al or Ti and O also confirmed the presence of a cracked layer. This could be because the sol-gel synthesis generates rapid condensation in sol, resulting in a shrinkage layer of gel film.[40] However, the EDX mapping of all catalysts exhibited that Pd was well dispersed on the catalyst supports layer as well as on the catalyst plate. It was noticed that Cr and Fe were detected due to their composition in the stainless-steel catalyst plate.

It was noted that the homogeneous catalyst layer was more favorable than cracking surface, which could be because the detachment of catalyst and substrate can occur during catalytic testing. However, some cracking might provide the benefit to improve the contacting area of catalyst and reactants if that cracking can attach to the substrate in catalytic testing environment.

XRD identified the crystallinity of catalyst. The XRD patterns of commercial Al_2O_3 powder, Pd/Al_2O_3 (SUS), and Pd/Al_2O_3 (SG) catalysts are shown in Fig. 6. The results showed that the crystalline structure of Pd/Al_2O_3 (SUS) exhibited main diffraction peaks at 2θ of 37.56º, 39.68º, 46.02º, 60.75º, and 67.12º, which represent gamma-alumina phase (ICDD 00-029-0063) in the indices of (311), (222), (400), (511), and (440) planes, respectively. Diffraction peaks at 33.87º, 54.90º, and 60.80º, which correspond to (100), (003), and (103) planes of the PdO phase (ICDD 01-075-0200) were also observed. The Pd/Al_2O_3 (SG) presented the main diffraction peaks of the gamma-alumina and PdO phase, similar to Pd/Al_2O_3 (SUS). Fig. 7 shows the XRD patterns of commercial nanopowder TiO_2, Pd/TiO_2 (SUS), and Pd/TiO_2 (SG). The Pd/TiO_2 (SUS) catalysts showed diffraction peaks at 25.29º, 36.95º, 37.82º, 38.59º, 48.02º, 53.90º, 55.04º, 62.72º, 68.92º, 70.28º, and 74.99º corresponding to the indices of anatase phase (ICDD 00-004-0477), which are (101), (103), (004), (112), (200), (105), (211), (204), (116), (220), and (215) planes respectively. Moreover, the Pd/TiO_2 (SUS) catalysts presented main diffraction peaks at 27.43º, 36.08º, 41.23º, 44.01º, 54.30º, 56.61º, 64.04º, 69.79º, and 76.02º indicating the indices of rutile phase (ICDD 00-004-0551), which are (110), (101), (111), (210), (211), (220), (310), (112), and (202) planes respectively. The crystalline structure of TiO_2 from Pd/TiO_2

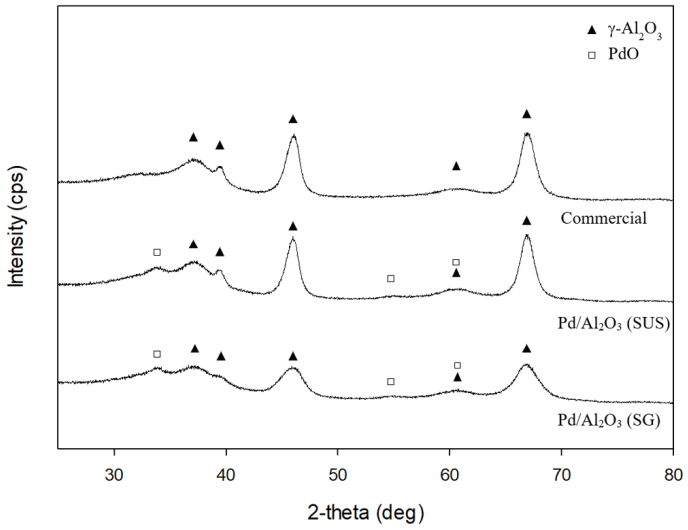

Fig. 6 – *XRD patterns of commercial Al_2O_3 powder and Pd/Al_2O_3 catalyst*

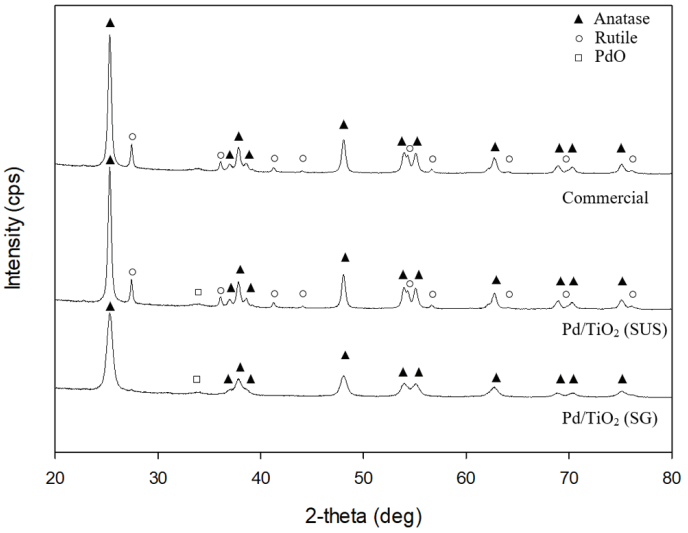

Fig. 7 – *XRD patterns of commercial TiO_2 powder and Pd/TiO_2 catalyst*

(SUS) showed the same nanopowder TiO_2 structure pattern, while the XRD pattern of the Pd/TiO_2 (SG) showed the crystalline structure of pure anatase phase.[41–43] The Pd showed diffraction peak at 33.87º, which referred to (100) plane of PdO phase. The BET surface areas of Pd/Al_2O_3 (SUS), Pd/Al_2O_3 (SG), Pd/TiO_2 (SUS), and Pd/TiO_2 (SG) catalysts are reported in Table 2. For both Al_2O_3- and TiO_2-supported catalysts, the one prepared by sol-gel gave a significantly higher surface area than the one prepared by the suspension. These results are in line with previous studies[41,44] showing a high surface area of support synthesized by sol-gel compared to support prepared by conventional synthesis.

The adhesion test results of all prepared catalysts are shown in Table 2. For Al_2O_3-supported catalysts, Pd/Al_2O_3 (SUS) and Pd/Al_2O_3 (SG) exhibited 83.05 and 82.74 % adhesion. For TiO_2-supported catalysts, Pd/TiO_2 (SUS) showed higher %adhesion, as compared to Pd/TiO_2 (SG). This could be because, during the coating steps, suspension slurries and Al_2O_3 sol solution were added with PVA binder, which could improve the adhesion between catalyst and catalyst plate. Hydroxyl group in PVA could enhance the interaction between the alumina particles by having hydrogen bond formation (Al–O–H$\cdots$OH or Al–O–$\cdots$OH). This hydrogen bond bridge could improve the adhesion for alumina coating.[39] On the other hand, Pd/TiO_2 (SG) exhibited much lower %adhesion as compared to the others. This could be due to the absence of binder in the coating solution, which resulted in an unstable cracked layer observed by SEM and 3D-optical profile image.

Catalyst activity testing for BHD production

The catalytic activity of the prepared Pd-supported catalysts was investigated in the deoxygenation of the palm oil process. The deoxygenation was performed in a microscale-based reactor for eight hours at 325 ºC and 3.4 MPa. These operating conditions were recommended by our industrial partner, and suggested as optimal by many published studies[45–47] for deoxygenation of triglycerides. WHSV (4.6–27.9 h^{-1}) and H_2/oil molar ratio of 96 were selected to obtain comparable conversions for the catalytic activity over the differently prepared catalysts as well as to support the slug flow microfluidic behavior in the microscale-based reactor.

Since the amounts of catalyst coated on the catalyst plate were not constant to keep the flow pattern the same for all experiments, the WHSV was varied, as shown in Table 2. Product yield per unit weight of catalyst or space-time yield (STY) was considered to evaluate catalyst performance among the catalysts tested.

Fig. 8 exhibits the catalytic activity, assessed through space-time yield, of different Pd-supported catalysts. For comparison, the catalytic activity was also illustrated in a spider chart together with the catalyst properties, as shown in Fig. 9. The results indicated that the conversion of palm oil over Pd/Al_2O_3 (SUS), Pd/Al_2O_3 (SG), and Pd/TiO_2 (SG) catalysts were overall very close to 100 % for eight hours on-stream. Triglycerides conversion slightly decreased after six hours for the Pd/TiO_2 (SUS) catalyst. The Pd/TiO_2 (SG) gave the highest space-time yield of BHD followed by Pd/TiO_2 (SUS), Pd/Al_2O_3 (SG), and Pd/Al_2O_3 (SUS), as shown in Fig. 8. The Pd/TiO_2 catalysts exhibited higher STY when compared to Pd/Al_2O_3 catalysts. This result illuminates the synergetic effect among Pd particles and titania support, which is described by the spillover mechanism. In the spillover mechanism, absorbed hydro-

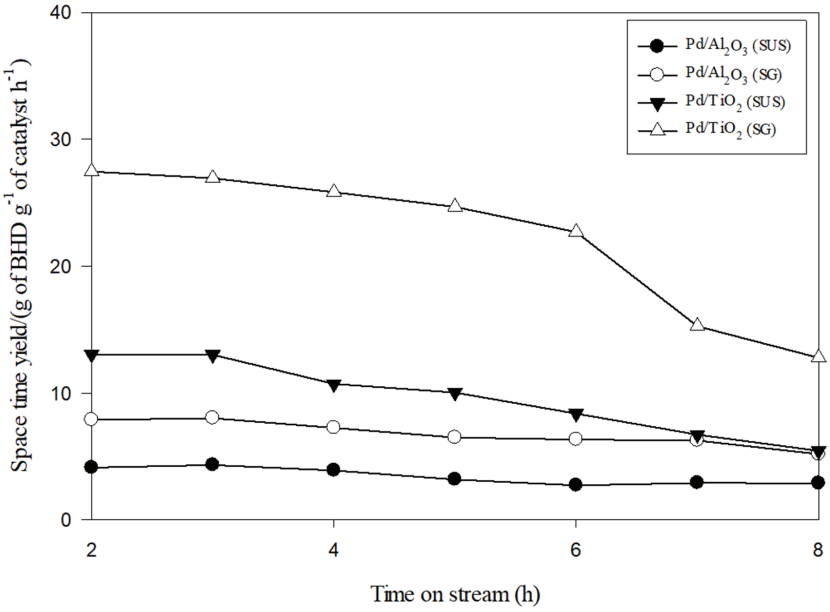

Fig. 8 – *Comparison of catalytic activity over different Pd-supported catalysts in terms of space-time yield (STY), as a function of time on stream (reaction condition: T = 325 °C, p = 3.4 MPa, H_2/feed molar ratio = 96)*

gen in the Pd nanoparticle diffuses into the titania support such that Ti^{4+} is reduced to Ti^{3+} Lewis acid sites. After the reduction, the oxygenated groups strongly interact with Ti^{3+}, leading to the weakening of the C=O bond and deoxygenation occurs.[48,49] The Pd/TiO_2 (SG) gave higher STY than the Pd/TiO_2 (SUS), which could be explained by a strong metal-support interaction (SMSI) effect. The Pd/TiO_2 (SG) contains a pure anatase phase, which generally shows the SMSI effect. In contrast, the Pd/TiO_2 (SUS) had a mixed phase of anatase and rutile that did not significantly express the SMSI effect at low reduction temperature.[33,48,50] The Pd/TiO_2 (SG) has a high surface area compared to Pd/TiO_2 (SUS). Higher surface area provides the opportunity for better metal dispersion on the catalyst surface. Also, some cracks of Pd/TiO_2 (SG) might increase diffusion in the catalyst layer, which helps catalyst performance before the catalyst is detached from the substrate.[38]

For Pd/Al_2O_3 catalysts, Pd/Al_2O_3 (SG) gave higher STY as compared to Pd/Al_2O_3 (SUS), which could be owing to the high surface area of the Pd/Al_2O_3 (SG) catalyst.

A brown precipitate was observed in the exit stream after a certain time on-stream. The precipitate was filtered and analyzed by SEM-EDX to investigate the catalyst deactivation. The result is shown in Table 3. The EDX results show that the precipitate contained Al, Ti, O, Fe, and Cr contents, indicating the detachment of catalyst and oxide layer of catalyst plate. The leaching of catalysts could result in the relatively lower STY after six hours of time on stream.

Table 4 shows conversions of a triglyceride feedstock and BHD yields over Pd/TiO_2 (SG) operating in a conventional fixed bed reactor and a microscale-based reactor. For a fixed bed reactor, a nearly complete conversion (96 %) was observed at WHSV of 2.0 h^{-1}, and only 63.6 % conversion[33] at WHSV of 2.7 h^{-1}. It is noteworthy that for fixed bed reactors, the operation at low space velocity is required to achieve a high BHD yield. On the other

Table 3 – *Element composition (wt%) of precipitate in liquid product*

Catalyst	Element/wt%				
	O	Al	Ti	Cr	Fe
Pd/Al_2O_3 (SUS)	45.39	1.06	–	1.27	52.28
Pd/Al_2O_3 (SG)	20.07	1.23	–	5.68	73.02
Pd/TiO_2 (SUS)	28.28	–	0.09	37.69	33.94
Pd/TiO_2 (SG)	19.37	–	0.34	0.77	79.52

Table 4 – *Catalytic activity of Pd/TiO_2 in fixed bed and microscale-based reactors*

	Conversion/%	BHD yield/%	STY/ (g BHD g^{-1} catalyst h^{-1})	WHSV/h^{-1}
Pd/TiO_2 (fixed bed)	96.0	47.3	0.7	2.0
Pd/TiO_2 (fixed bed)[33]	63.6	39.2	1.0	2.7
Pd/TiO_2 (SG-Microreactor)	100.0	79.0	22.7	27.9

*At TOS = 6 h

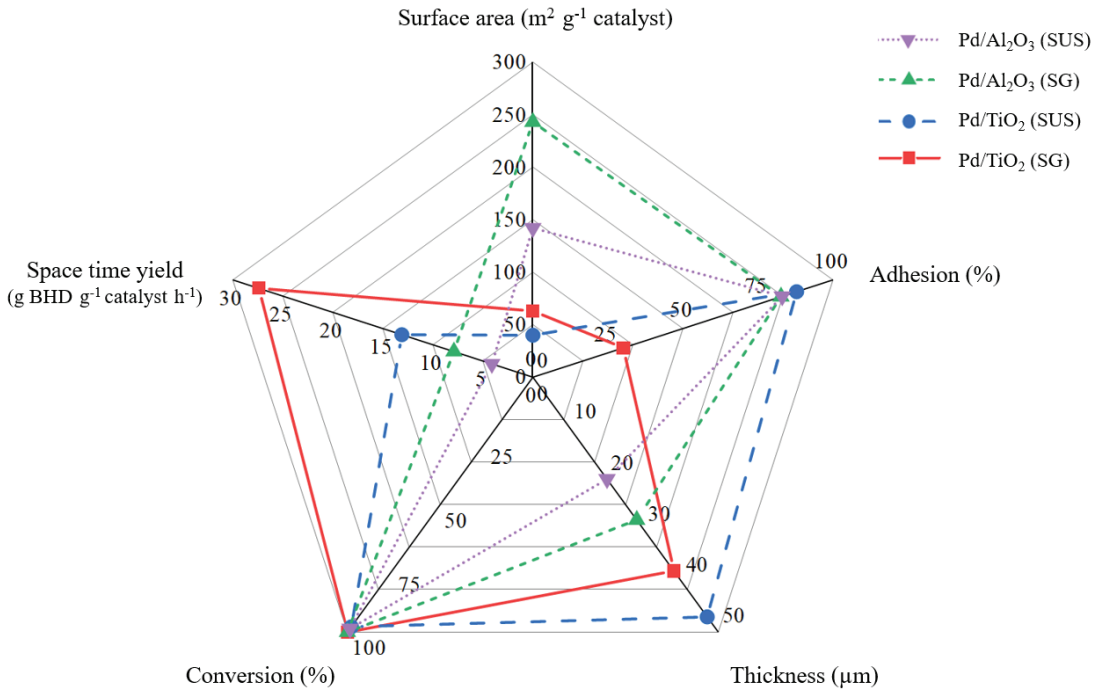

Fig. 9 – *Spider diagram of Pd/Al_2O_3 (SUS), Pd/Al_2O_3 (SG), Pd/TiO_2 (SUS), and Pd/TiO_2 (SG)*

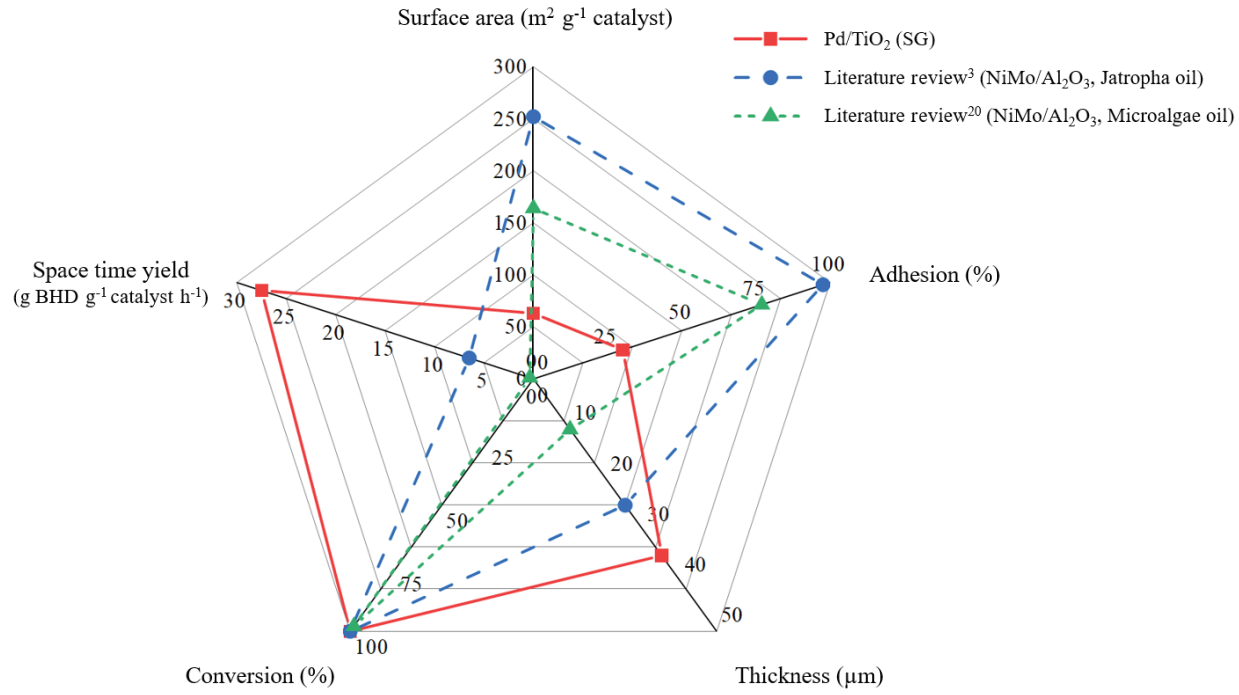

Fig. 10 – *Comparison of Pd/TiO_2 (SG) catalyst performance with catalysts[3,20] performing similar chemical reaction process*

hand, a microscale-based reactor exhibits a complete conversion (100 %) with high STY at a higher space velocity of 27.9 h^{-1}. These experimental results illustrate that operations in microscale-based reactors are superior to packed bed performance. Fundamental analysis[34,35] and our experimental results prove that due to its excellent mass transfer, the contact time for the deoxygenation reaction could be substantially reduced. Thus, microscale-based reactors provide higher productivity for the BHD process as compared to conventional fixed bed reactors.

It is interesting to compare the performance of our arguably best catalyst Pd/TiO_2 (SG) with catalysts used in similar reaction processes with Jatropha[3] and Microalgae[20] oil.

Fig. 10 shows the catalyst properties and catalytic performance of the Pd/TiO_2 (SG) compared to two literature studies. The first study, Sinha *et al.*, investigated the deoxygenation of jatropha oil over presulfided $NiMo/Al_2O_3$ in microreactor to produce BHD and jet fuel at 380 °C, 3.8 MPa, and H_2/feed ratio of 2,500 NL L^{-1}, WHSV of 46 h^{-1}.[2] The other study, *Zhou et al.*, investigated the deoxygenation of microalgae oil over presulfided $NiMo/Al_2O_3$ in microreactor for BHD production at 360 °C, 3.4 MPa, H_2/oil ratio of 1,000 mL mL^{-1}, WHSV of 0.65 h^{-1}.[9] All reaction processes were performed in microscale-based reactors and yielded alike BHD products.

As shown in the diagram, all studies exhibited complete conversion, while this study presented the highest STY of BHD product. The Pd/TiO_2 (SG) exhibited the lowest surface area and degree of adhesion, and the highest thickness of catalyst layer as compared to the others. High space-time yield obtained with our Pd/TiO_2 (SG) catalyst implies promising overall process performance results. The relatively lower surface area of TiO_2 support as compared to Al_2O_3 still provides enough active sites for the reaction. The low degree of adhesion was presented in Pd/TiO_2 (SG), which could be due to the high thickness of catalyst, surface cracking, and no additive in coating process.

Obviously, specific surface area (m^2 g^{-1} catalyst) and adhesion properties of Pd/TiO_2 (SG) could be improved to create a truly superior catalyst for BHD production from plant-based triglycerides.

Conclusions

Pd/Al_2O_3 and Pd/TiO_2 catalysts with suspension and sol-gel coating methods were investigated for biohydrogenated diesel production in a microscale-based reactor. The SEM and 3D optical profile images indicated that the coating by suspension slurry provided a homogeneous catalyst layer, while the coating by sol-gel solution provided a non-homogeneous layer. In the adhesion test, the Pd/TiO_2 (SG) showed the lowest %adhesion due to the absence of PVA binder and the presence of a cracked non-homogeneous layer. The Pd/Al_2O_3 (SUS), Pd/Al_2O_3 (SG), and Pd/TiO_2 (SG) catalysts exhibited conversions closed to 100 %. For the Pd/TiO_2 (SUS) catalyst, the conversion slightly decreased because of its low surface area. The highest space-time yield of BHD was obtained by Pd/TiO_2 (SG), which was due to the presence of pure anatase phase that strongly interacted with Pd, thus promoting the hydrogen spillover effect for the deoxygenation reaction. Despite low adhesion and coating non-uniformity, Pd/TiO_2 (SG) provided the highest catalytic performance for deoxygenation reaction. The reaction process in the microscale-based reactor exhibited a much higher space-time yield, when compared to classic fixed bed operation, due to its superior mass transfer. However, improved adhesion of the coated catalyst should be further developed. It could be concluded that Pd/TiO_2 (SG) coating was successful in deoxygenation of triglyceride application in microscale-based reactor.

ACKNOWLEDGMENTS

The authors acknowledge Research and Researcher for Industry (RRi), Ph.D. program (Grant No. PHD60I0025), the Thailand Research Fund (TRF); the Petroleum and Petrochemical College, Chulalongkorn University; Center of Excellence on Petrochemical and Materials Technology; and Innovation Institute, PTT Public Company Limited for the financial support.

References

1. *Kiwi-Minsker, L., Renken, A.*, Microstructured reactors for catalytic reactions, Catal. Today **110** (2005) 2. doi: https://doi.org/10.1016/j.cattod.2005.09.011
2. *Plutschack, M. B., Pieber, B., Gilmore, K., Seeberger, P. H.*, The Hitchhiker's guide to flow chemistry, Chem. Rev. **117** (2017) 11796. doi: https://doi.org/10.1021/acs.chemrev.7b00183
3. *Sinha, A. K., Sibi, M. G., Naidu, N., Farooqui, S. A., Anand, M., Kumar, R.*, Process intensification for hydroprocessing of vegetable oils: Experimental study, Ind. Eng. Chem. Res. **53** (2014) 19062. doi: https://doi.org/10.1021/ie502703z
4. *Yao, X., Zhang, Y., Du, L., Liu, J., Yao, J.*, Review of the applications of microreactors, Renewable Sustainable Energy Rev. **47** (2015) 519. doi: https://doi.org/10.1016/j.rser.2015.03.078
5. *Deng, J., Zhang, J., Wang, K., Luo, G.*, Microreaction technology for synthetic chemistry, Chin. J. Chem. **37** (2019) 161. doi: https://doi.org/10.1002/cjoc.201800428
6. *De Risi, C., Bortolini, O., Brandolese, A., Di Carmine, G., Ragno, D., Massi, A.*, Recent advances in continuous-flow organocatalysis for process intensification, React. Chem. Eng. **5** (2020) 1017. doi: https://doi.org/10.1039/D0RE00076K

7. *Yan, Z., Tian, J., Wang, K., Nigam, K. D. P., Luo, G.*, Microreaction processes for synthesis and utilization of epoxides: A review, Chem. Eng. Sci. **229** (2021) 116071. doi: https://doi.org/10.1016/j.ces.2020.116071
8. *Joshi, N., Lawal, A.*, Hydrodeoxygenation of acetic acid in a microreactor, Chem. Eng. Sci. **84** (2012) 761. doi: https://doi.org/10.1016/j.ces.2012.09.018
9. *Ahn, G. N., Yu, T., Lee, H. J., Gyak, K. W., Kang, J. H., You, D., Kim, D. P.*, A numbering-up metal microreactor for the high-throughput production of a commercial drug by copper catalysis, Lab Chip **19** (2019) 3535. doi: https://doi.org/10.1039/C9LC00764D
10. *Bojang, A. A., Wu, H. S.*, Design, fundamental principles of fabrication and applications of microreactors, Processes **8** (2020) 891. doi: https://doi.org/10.3390/pr8080891
11. *Santacesaria, E., Di Serio, M., Tesser, R., Turco, R., Tortorelli, M., Russo, V.*, Biodiesel process intensification in a very simple microchannel device, Chem. Eng. Process. **52** (2012) 47. doi: https://doi.org/10.1016/j.cep.2011.12.001
12. *Venvik, H. J., Yang, J.*, Catalysis in microstructured reactors: Short review on small-scale syngas production and further conversion into methanol, DME and Fischer-Tropsch products, Catal. Today **285** (2017) 135. doi: https://doi.org/10.1016/j.cattod.2017.02.014
13. *Yue, J.*, Multiphase flow processing in microreactors combined with heterogeneous catalysis for efficient and sustainable chemical synthesis, Catal. Today **308** (2018) 3. doi: https://doi.org/10.1016/j.cattod.2017.09.041
14. *Montebelli, A., Visconti, C. G., Groppi, G., Tronconi, E., Cristiani, C., Ferreira, C., Kohler, S.*, Methods for the catalytic activation of metallic structured substrates, Catal. Sci. Technol. **4** (2014) 2846. doi: https://doi.org/10.1039/C4CY00179F
15. *Jähnisch, K., Hessel, V., Löwe, H., Baerns, M.*, Chemistry in microstructured reactors, Angew. Chem. Int. Ed. **43** (2004) 406. doi: https://doi.org/10.1002/anie.200300577
16. *Aghel, B., Mohadesi, M., Sahraei, S.*, Effect of different cosolvents on transesterification of waste cooking oil in a microreactor, Chem. Eng. Technol. **41** (2018) 598. doi: https://doi.org/10.1002/ceat.201700025
17. *Mohadesi, M., Aghel, B., Maleki, M., Ansari, A.*, Study of the transesterification of waste cooking oil for the production of biodiesel in a microreactor pilot: The effect of acetone as the co-solvent, Fuel **273** (2020) 117736. doi: https://doi.org/10.1016/j.fuel.2020.117736
18. *Zheng, Y., Shadloo, M. S., Nasiri, H., Maleki, A., Karimipour, A., Tlili, I.*, Prediction of viscosity of biodiesel blends using various artificial model and comparison with empirical correlations, Renewable Energy **153** (2020) 1296. doi: https://doi.org/10.1016/j.renene.2020.02.087
19. *Madhawan, A., Arora, A., Das, J., Kuila, A., Sharma, V.*, Microreactor technology for biodiesel production: A review, Biomass Convers. Biorefin. **8** (2018) 485. doi: https://doi.org/10.1007/s13399-017-0296-0
20. *Zhou, L., Lawal, A.*, Evaluation of presulfided NiMo/γ-Al_2O_3 for hydrodeoxygenation of microalgae oil to produce green diesel, Energy Fuels **29** (2015) 262. doi: https://doi.org/10.1021/ef502258q
21. *Zhou, L., Lawal, A.*, Hydrodeoxygenation of microalgae oil to green diesel over Pt, Rh and presulfided NiMo catalysts, Catal. Sci. Technol. **6** (2016) 1442. doi: https://doi.org/10.1039/C5CY01307K
22. *Zhou, L., Lawal, A.*, Kinetic study of hydrodeoxygenation of palmitic acid as a model compound for microalgae oil over Pt/γ-Al_2O_3, Appl. Catal. A **532** (2017) 40. doi: https://doi.org/10.1016/j.apcata.2016.12.014
23. *Ying, X., Zhang, L., Xu, H., Ren, Y. L., Luo, Q., Zhu, H. W., Qu, H., Xuan, J.*, Efficient Fischer–Tropsch microreactor with innovative aluminizing pretreatment on stainless steel substrate for Co/Al_2O_3 catalyst coating, Fuel Process. Technol. **143** (2016) 51. doi: https://doi.org/10.1016/j.fuproc.2015.11.005
24. *Meille, V.*, Review on methods to deposit catalysts on structured surfaces, Appl. Catal. A **315** (2006) 1. doi: https://doi.org/10.1016/j.apcata.2006.08.031
25. *Haas-Santo, K., Görke, O., Pfeifer, P., Schubert, K.*, Catalyst coatings for microstructure reactors, Chimia **56** (2002) 605. doi: https://doi.org/10.2533/000942902777679993
26. *Sohrabi, S., Keshavarz Moraveji, M., Iranshahi, D.*, A review on the design and development of photocatalyst synthesis and application in microfluidic reactors: Challenges and opportunities, Rev. Chem. Eng. **36** (2020) 687. doi: https://doi.org/10.1515/revce-2018-0013
27. *Schmidt, S. A., Kumar, N., Zhang, B., Eränen, K., Murzin, D. Y., Salmi, T.*, Preparation and characterization of alumina-based microreactors for application in methyl chloride synthesis, Ind. Eng. Chem. Res. **51** (2012) 4545. doi: https://doi.org/10.1021/ie202922x
28. *Truyen, D., Courty, M., Alphonse, P., Ansart, F.*, Catalytic coatings on stainless steel prepared by sol–gel route, Thin Solid Films **495** (2006) 257. doi: https://doi.org/10.1016/j.tsf.2005.08.200
29. *Bahuguna, G., Mishra, N. K., Chaudhary, P., Kumar, A., Singh, R.*, Thin film coating through sol-gel technique, Res. J. Chem. Sci. **6** (2016) 65.
30. *Kiatkittipong, W., Phimsen, S., Kiatkittipong, K., Wongsakulphasatch, S., Laosiripojana, N., Assabumrungrat, S.*, Diesel-like hydrocarbon production from hydroprocessing of relevant refining palm oil, Fuel Process. Technol. **116** (2013) 16. doi: https://doi.org/10.1016/j.fuproc.2013.04.018
31. *Zhong, H., Xianqin, W.*, Hydrodeoxygenation of model compounds and catalytic systems for pyrolysis bio-oils upgrading, Catal. Sustainable Energy **1** (2012) 28. doi: https://doi.org/10.2478/cse-2012-0004
32. *Echeandia, S., Pawelec, B., Barrio, V. L., Arias, P. L., Cambra, J. F., Loricera, C. V., Fierro, J. L. G.*, Enhancement of phenol hydrodeoxygenation over Pd catalysts supported on mixed HY zeolite and Al_2O_3. An approach to O-removal from bio-oils, Fuel **117** (2014) 1061. doi: https://doi.org/10.1016/j.fuel.2013.10.011
33. *Hengsawad, T., Jindarat, T., Resasco, D. E., Jongpatiwut, S.*, Synergistic effect of oxygen vacancies and highly dispersed Pd nanoparticles over Pd-loaded TiO_2 prepared by a single-step sol–gel process for deoxygenation of triglycerides, Appl. Catal. A **566** (2018) 74. doi: https://doi.org/10.1016/j.apcata.2018.08.007
34. *Kordouli, E., Sygellou, L., Kordulis, C., Bourikas, K., Lycourghiotis, A.*, Probing the synergistic ratio of the NiMo/γ-Al_2O_3 reduced catalysts for the transformation of natural triglycerides into green diesel, Appl. Catal. B **209** (2017) 12. doi: https://doi.org/10.1016/j.apcatb.2017.02.045
35. *Srifa, A., Faungnawakij, K., Itthibenchapong, V., Assabumrungrat, S.*, Roles of monometallic catalysts in hydrodeoxygenation of palm oil to green diesel, Chem. Eng. J. **278** (2015) 249. doi: https://doi.org/10.1016/j.cej.2014.09.106

36. *Behravesh, E., Kilpiö, T., Russo, V., Eränen, K., Salmi, T.*, Experimental and modelling study of partial oxidation of ethanol in a micro-reactor using gold nanoparticles as the catalyst, Chem. Eng. Sci. **176** (2018) 421. doi: https://doi.org/10.1016/j.ces.2017.11.011
37. *Laguna, O. H., Domínguez, M. I., Centeno, M. A., Odriozola, J. A.,* New materials for catalytic applications, Elsevier, Amsterdam, 2016, pp 81-120. doi: https://doi.org/10.1016/B978-0-444-63587-7.00004-4
38. *Erfan, B., Kari, E., Narendra, K., Janne, P., Markus, P., Atte, A., Mari, N., Martti, T., Yu, M. D., Tapio, S.*, Microreactor coating with Au/Al_2O_3 catalyst for gas-phase partial oxidation of ethanol: Physico-chemical characterization and evaluation of catalytic properties, Chem. Eng. J. **378** (2019) 122179. doi: https://doi.org/10.1016/j.cej.2019.122179
39. *He, L., Fan, Y., Luo, L., Bellettre, J., Yue, J.*, Preparation of $Pt/\gamma\text{-}Al_2O_3$ catalyst coating in microreactors for catalytic methane combustion, Chem. Eng. J. **380** (2020) 122424. doi: https://doi.org/10.1016/j.cej.2019.122424
40. *Haas-Santo, K., Fichtner, M., Schubert, K.*, Preparation of microstructure compatible porous supports by sol–gel synthesis for catalyst coatings, Appl. Catal. A **220** (2001) 79. doi: https://doi.org/10.1016/S0926-860X(01)00714-1
41. *Liu, T. X., Liu, Y., Zhang, Z. J., Li, F. B., Li, X. Z.*, Comparison of aqueous photoreactions with TiO_2 in its hydrosol solution and powdery suspension for light utilization, Ind. Eng. Chem. Res. **50** (2011) 7841. doi: https://doi.org/10.1021/ie102584j
42. *Liu, H., Zhang, Y., Yang, H., Xiao, W., Sun, L.*, Study on synthesis and photocatalytic activity of porous titania nanotubes, Adv. Mater. Sci. Eng. **2016** (2016) 3532817. doi: https://doi.org/10.1155/2016/3532817
43. *Sakulkhaemaruethai, S., Suzuki, Y., Yoshikawa, S.*, Surfactant-assisted preparation and characterization of mesoporous titania nanocrystals, J. Ceram. Soc. Jpn. **112** (2004) 547. doi: https://doi.org/10.2109/jcersj.112.547
44. *Samain, L., Jaworski, A., Edén, M., Ladd, D. M., Seo, D. K., Javier Garcia-Garcia, F., Häussermann, U.*, Structural analysis of highly porous $\gamma\text{-}Al_2O_3$, J. Solid State Chem. **217** (2014) 1. doi: https://doi.org/10.1016/j.jssc.2014.05.004
45. *Sotelo-Boyás, R., Trejo-Zárraga, F., Hernández-Loyo, de Jesús Hernández-Loyo, F.,* Hydrogenation, IntechOpen, 2012. doi: https://doi.org/10.5772/48710
46. *Zhao, X., Wei, L., Cheng, S., Julson, J.*, Review of heterogeneous catalysts for catalytically upgrading vegetable oils into hydrocarbon biofuels, Catalysts **7** (2017) 83. doi: https://doi.org/10.3390/catal7030083
47. *Khan, S., Kay Lup, A. N., Qureshi, K. M., Abnisa, F., Wan Daud, W. M. A., Patah, M. F. A.*, A review on deoxygenation of triglycerides for jet fuel range hydrocarbons, J. Anal. Appl. Pyrolysis **140** (2019) 1. doi: https://doi.org/10.1016/j.jaap.2019.03.005
48. *Oi, L. E., Choo, M. Y., Lee, H. V., Ong, H. C., Hamid, S. B. A., Juan, J. C.*, Recent advances of titanium dioxide (TiO_2) for green organic synthesis, RSC Adv. **6** (2016) 108741. doi: https://doi.org/10.1039/C6RA22894A
49. *Prins, R.*, Hydrogen spillover. Facts and fiction, Chem. Rev. **112** (2012) 2714. doi: https://doi.org/10.1021/cr200346z
50. *Bagheri, S., Julkapli, N. M., Hamid, S. B. A.*, Titanium dioxide as a catalyst support in heterogeneous catalysis, Sci. World J. **2014** (2014) 1. doi: https://doi.org/10.1155/2014/727496